Journal of Synchrotron Radiation

Editors: Å. Kvick, D. M. Mills and T. Ohta
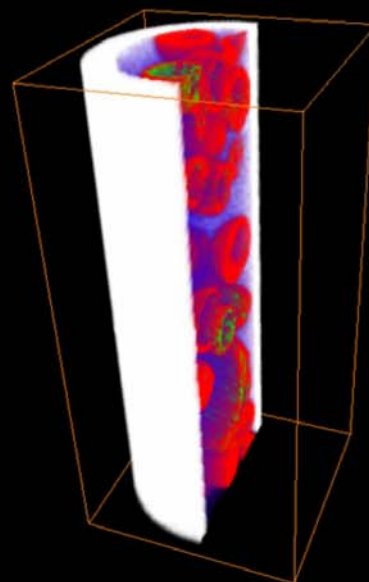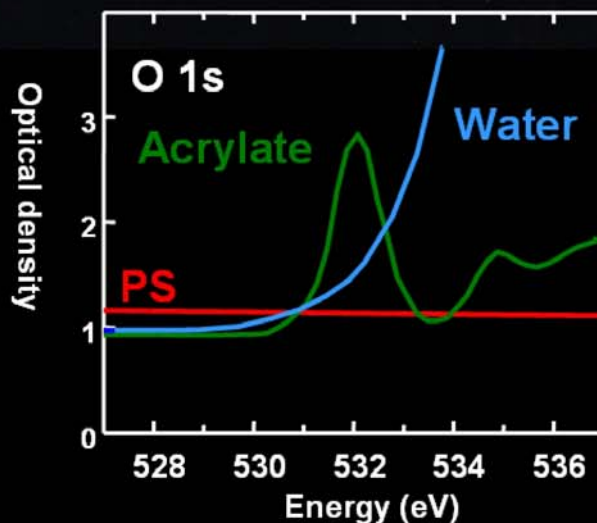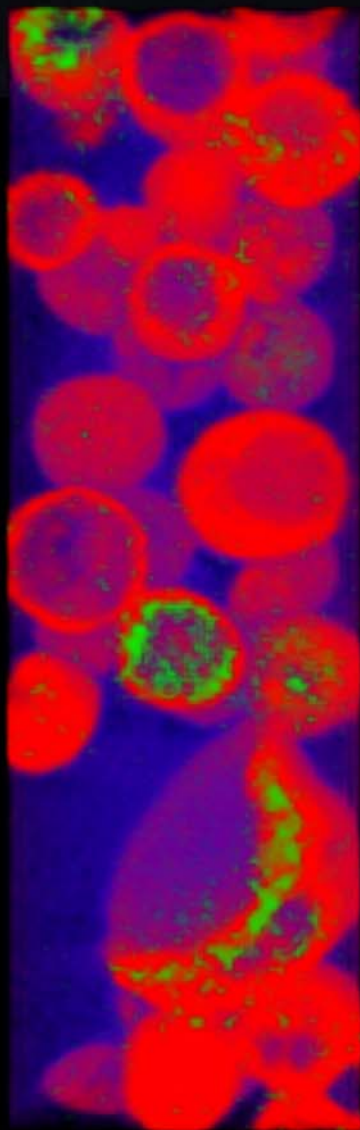
Göran A. Johansson, Tolek Tyliszczak, Gary Mitchell, Melinda Keefe and Adam P. Hitchcock

Three dimensional chemical mapping by scanning transmission X-ray spectromicroscopy

Three-dimensional chemical mapping by scanning transmission X-ray spectromicroscopy

Göran A. Johansson,[a]* Tolek Tyliszczak,[b] Gary E. Mitchell,[c] Melinda H. Keefe[d] and Adam P. Hitchcock[a]

[a]Department of Chemistry and BIMR, McMaster University, Hamilton, Canada L8S 4M1, [b]Advanced Light Source, LBNL, Berkeley, CA 94720, USA, [c]Analytical Sciences, The Dow Chemical Company, 1897 Building, Midland, MI 48667, USA, and [d]Dow Latex, The Dow Chemical Company, 1604 Building, Midland, MI 48674, USA. E-mail: gajohansson@lbl.gov

Three-dimensional (3-d) chemical mapping using angle-scan tomography in a scanning transmission X-ray microscope is demonstrated. Apparatus, experimental procedures and data processing are presented and the 3-d spatial resolution is evaluated. The technique is illustrated using mapping of a low-density acrylate polyelectrolyte in and outside of polystyrene microspheres dispersed in water in a 4 µm-diameter microcapillary. The 3-d chemical visualization provides information about the microstructure that had not previously been observed.

1. Introduction

Many chemical systems, whether they are of natural or synthetic origin, have a complex nanoscale structure and their functional characteristics depend heavily on it. Understanding the relationship between three-dimensional (3-d) chemical phase structure and critical material properties is necessary to predict and design materials. Yet, most chemical imaging studies are conducted as two-dimensional (2-d) projections. A method to visualize the detailed 3-d chemical structure at high spatial resolution will clearly be useful to further our understanding of complex nanoscale processing.

Hollow latex particles are a class of materials prepared by multi-stage emulsion polymerization techniques (Pavlyuchenko *et al.*, 2001; McDonald & Devon, 2002). These latexes have been developed for a variety of applications including architectural coatings as opacifying agents, paper coating as glossing aids, sunscreens as UV radiation absorption aids, and for controlled release processes (Kowalski *et al.*, 1984; Lee *et al.*, 1992; Jones *et al.*, 1997; Clikeman *et al.*, 1999; Blankenship, 2001). The hollow particle structure can be designed with interiors that vary from highly dense, with polymer struts in the void interior, to completely hollow (Beach *et al.*, 2005). The materials analyzed in this instance are polystyrene microspheres. Changes in their fine structure which result from variations in the process conditions significantly impact the performance of the final product. Methods to image the internal structure of such latex particles are thus needed to optimize processing.

Methods used for characterizing chemical and spatially differentiated latex particles have included electron micro-scopy (Stubbs & Sundberg, 2004; Beach *et al.*, 2005) and soft X-ray scattering (Araki *et al.*, 2006). While the structure in the dried state has been characterized by combining focused ion beam milling with scanning electron microscopy (Beach *et al.*, 2005), visualizing the structure in the wet state is more difficult. Structural changes which may occur during the drying process include particle shrinkage, precipitation of acrylic polyelectrolyte, and deformation of the spherical structure. In the case of electron microscopy, chemical imaging has also required that the samples are dried and treated with heavy metal stains. To understand the changes brought about by drying, one needs to understand the structure in the wet state. X-ray microscopy provides an opportunity to analyze 3-d compositional information on the latexes in the wet state prior to drying.

In recent years, a number of new methods have been developed to perform 3-d chemical mapping, including serial section scanning transmission X-ray microscopy (STXM) (Hitchcock *et al.*, 2003), focused ion beam milling combined with scanning electron microscopy (FIB-SEM) (Kotula *et al.*, 2004; Drohne *et al.*, 2005), and energy-filtered transmission electron microscopy (EF-TEM) (Möbus & Inkson, 2001; Weyland & Midgley, 2003). However, none of these methods have the spectroscopic resolution of the method presented here, nor the ability to analyze wet specimens. Previous soft X-ray microtomography experiments have been performed using STXM (Wang *et al.*, 2000) and full-field transmission X-ray microscopy (TXM) (Weiß *et al.*, 2000; Larabell & Le Gros, 2004; Le Gros *et al.*, 2005). However, in all cases to date, only a single photon energy was used. These studies, typically on biological samples, have provided high-spatial-resolution

doi:10.1107/S0909049507029962 **395**

density-based images of wet samples, but no direct spectroscopic-based chemical information. Near-edge X-ray absorption fine-structure spectroscopy (NEXAFS) performed using soft X-ray STXM has a high degree of chemical sensitivity (Ade, 1998; Ade & Urquhart, 2002). As a photon-in/photon-out technique, it is well suited for analyzing samples in hydrated environments (Hitchcock, Morin et al., 2005; Lawrence et al., 2003; Dynes, Lawrence et al., 2006; Dynes, Tyliszczak et al., 2006). Thus, the combination of NEXAFS to achieve chemical sensitivity, and tomography with submicrometer spatial resolution performed using STXM shows great potential when applied to chemical systems, such as multiphase polymer composites (Hitchcock, Stöver et al., 2005), biomineralization, soil samples, biomaterials (Hitchcock et al., 2003) etc. Although the majority of STXM studies to date have involved 2-d projections, there are two previous cases where 3-d imaging was performed in STXM. Wang et al. (2000) have reported a tour de force cryotomography measurement consisting of images at 24 angles (-55 to $60°$) of a 40 µm $\times$ 30 µm region of mouse 3T3 fibroblast cells at a single photon energy (520 eV). However, their measurements were restricted to only a single photon energy [as are most full-field tomography studies (Weiß et al., 2000; Larabell & Le Gros, 2004)] and thus the contrast was primarily density rather than chemical in nature. The only previous 3-d imaging study using chemical contrast was that reported by Hitchcock et al. (2003) using a serial sectioning technique in STXM, and imaging at multiple energies in the C 1s region, to generate 3-d maps of the chemical components of toner particles.

Here we report on the development of methods for applying computed angle-scan tomography in a scanning transmission X-ray microscope at multiple photon energies for chemical visualization. The goal is to perform X-ray tomography at a spatial resolution in all three dimensions of better than 50 nm, while simultaneously using the capability of STXM to acquire NEXAFS signals over a 3-d volume at very high spectral resolution. This allows identification and quantification of the chemical composition of the sample in a spatial volume. In this study we present our experimental arrangement, sample preparation, measurement procedures and results of STXM-based 'chemical tomography'. Chemical maps of acrylate polyelectrolyte-filled polystyrene microspheres derived from the 3-d volume are shown to illustrate the capabilities of our current implementation, and provide a platform to discuss the ultimate potential of this technique.

2. Experimental methods

2.1. STXM and NEXAFS

X-ray imaging and spectroscopy were carried out using the scanning transmission X-ray microscope at beamline 5.3.2 (Warwick et al., 2002; Kilcoyne et al., 2003) of the Advanced Light Source (ALS). STXM is a synchrotron-based analytical microscopy (Ade, 1998; Ade & Urquhart, 2002) which achieves strong chemical sensitivity through NEXAFS contrast (Stöhr, 1992). It can provide quantitative maps of

chemical species at environmentally relevant concentrations (i.e. mg kg^{-1} global), with a spatial resolution of better than 50 nm (Lawrence et al., 2003; Dynes, Lawrence et al., 2006; Dynes, Tyliszczak et al., 2006). In the implementation at the ALS 5.3.2 bending-magnet beamline used in this work, STXM provides excellent spectroscopy in the soft X-ray regions with more than 3000 resolving power over a photon energy range from 200 to 600 eV. It also has the ability to achieve a spatial resolution of better than 40 nm over the full range of accessible photon energies through the use of differential laser interferometers. Recording images at X-ray energies at which specific compounds absorb preferentially provides a means for locating specific compounds. A much more powerful technique is to record a full image sequence ('stack'; Jacobsen et al., 2000) and then fit the spectrum at each pixel to a set of quantitative reference spectra to extract quantitative chemical maps (Hitchcock, Morin et al., 2005; Lawrence et al., 2003; Dynes, Lawrence et al., 2006; Dynes, Tyliszczak et al., 2006). When this type of image sequence measurement is carried out at a fine mesh of angles, in a computed angle-scan tomography experiment, the resulting four-dimensional (4-d) data set (x, y, E, θ) can be used to generate a quantitative 3-d map of each chemical species present in the sampled volume. While this is the ultimate goal of this project, in fact only two photon energies were used, which is sufficient to map what is essentially a two-component system. The results presented here emphasize the methods for data reduction, evaluation of the performance, and demonstration of the value added from chemical information derived from multi-energy tomograms. A future work will report results in which a many-energy stack is recorded at each angle.

2.2. Sample preparation

Glass capillaries were used to hold the sample and keep it hydrated. These glass capillaries are similar to the ones typically used in intra- and extra-cellular physiology as micropipettes to study electrical activity in cells and for injecting a variety of substances (Jurkat-Rott & Lehmann-Horn, 2004). To create a hollow tip with micrometer dimensions, the capillaries (initial diameter of 1 mm) were heated and pulled using a micropipette puller (P-87 Flaming/Brown Micropipette Puller, Sutter Instruments Inc., Novato, CA, USA). For the STXM tomography experiment, the pulling parameters were chosen so that the tip diameter would be 2–5 µm and have a uniform thickness over the imaged length, 10–20 µm. The thickness of the glass wall of the tip is a few hundred nanometers.

The hollow latex particles investigated were obtained as a polymer colloidal dispersion in water with 30% polymer solids. In the wet state the hollow particles have a rigid polystyrene (PS) shell and a polyacrylate water solution in the core. After drying, the water evaporates through the shell resulting in hollow particles of approximately 1 µm outer diameter and 50% void fraction. The polymer colloidal dispersion was diluted with distilled de-ionized water to 1 part in 10000, and then a syringe was used to force the particles into

the very fine tip of the glass capillary. Both ends of the capillary were then sealed with silicone grease.

2.3. Tomographic data-acquisition procedures

Tomography requires collection of multiple 2-d images over as wide a range of projection angles as possible to achieve a reconstruction without severe artifacts (Baumeister *et al.*, 1999). By using a capillary to hold the sample, the symmetrical cylindrical geometry of the capillary allows the sample to be oriented over the full 360°. A special sample stage (see Fig. 1) was developed to rotate the glass capillary containing the sample perpendicular to the X-ray beam inside the STXM. The tomography sample stage uses an ARSAPE two-phase stepper motor (AM1020-A-0,25-8) and a Newport ESP7000 Universal Motion Controller to rotate the capillary. The use of this stage required the sample be repositioned and refocused for every angle. Work is currently under way to construct a eucentric sample-mounting stage that can adjust the sample more precisely to the rotation axis, which will reduce or eliminate the need for repositioning and refocusing of the sample for each projection and thus speed up data collection.

A tomographic data set was acquired by taking images at the two energies (530.0, 532.2 eV) from 0 to 180° rotation angles, at 3° increments. At each angle the sample was repositioned and focused manually by the microscope operator, before acquiring data.

2.4. Data processing: alignment, sectioning and presentation

Fig. 2 shows a flow diagram of the data processing. The initial image and spectral processing was carried out using
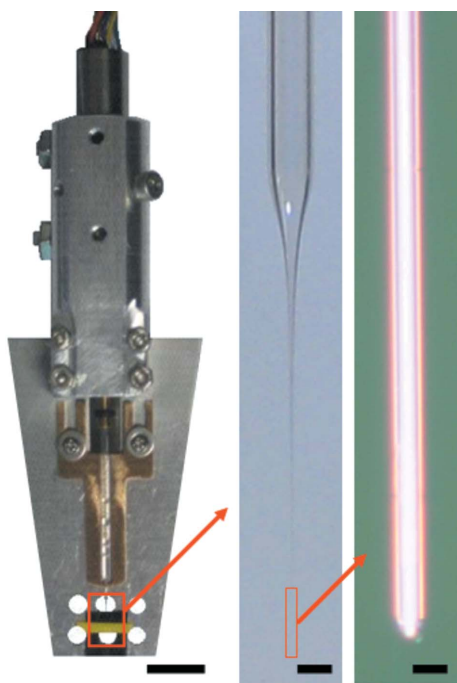

Figure 2
Flow chart for acquisition and processing the STXM tomography data.

aXis2000 software[1] which can handle the 4-d data stacks (2-d spatial, spectral and tilt angle) acquired by the STXM. All images are transformed into an optical density (OD) scale, $OD = -\ln(I/I_0)$, where I is the intensity of the transmitted X-rays and I_0 is the intensity of the incident X-rays. This transformation normalizes for the variation in the X-ray beam during data acquisition and enables better estimates of the sample thickness in various regions.

The images from a selected single energy or from energy-difference chemical maps can be organized as a 3-d image projection data set. After the initial processing from as-recorded data to OD images or difference maps using *aXis2000*, the projection series (data at all rotation angles) is exported to the MRC file format (Crowther *et al.*, 1996) which can be imported by many major electron microscopy tomography reconstruction programs. Currently, the *IMOD* software (Kremer *et al.*, 1996; Mastronarde, 1997) package is being used, which is available free from the Boulder Laboratory for 3-d Electron Microscopy, University of Colorado, USA. *IMOD* can perform alignment of projection series to a common axis of rotation by autocorrelation and/or alignment to fiducial markers. The alignment can be visualized as a sinogram (Johansson *et al.*, 2006b) which gives a good indication of the quality of the alignment. Finally, a 3-d volume reconstruction can be performed using filtered back projection.

Figure 1
Left: photograph of the tomography rotation stage with plate used to support the rotation structure in the STXM kinematic mount (scale bar 10 mm). Middle: a close-up of the glass capillary (scale bar 1 mm). Right: the fine tip of an empty capillary (scale bar = 5 μm).
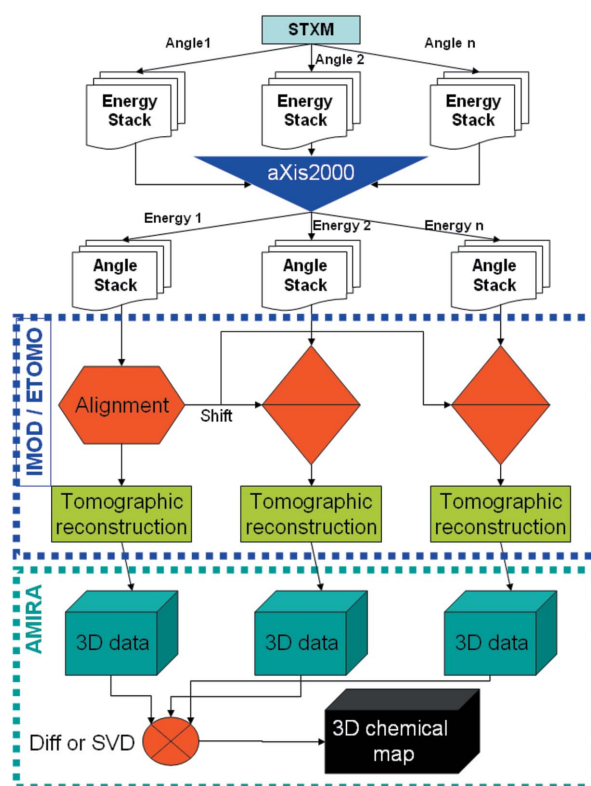
---

[1] *aXis200* is written in Interactive Data Language (IDL). It is available free for non-commercial use from http://unicorn.mcmaster.ca/aXis2000.html.
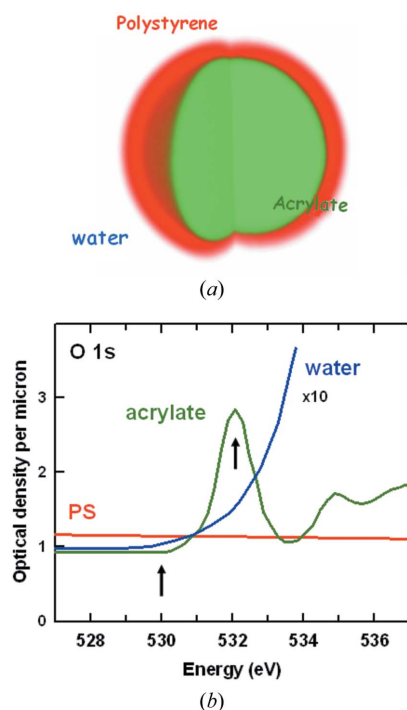
Figure 3
(*a*) Schematic of the acrylate polyelectrolyte-filled microsphere sample. (*b*) NEXAFS spectra of polystyrene (PS) and polyacrylate in the region below the onset of strong O 1*s* absorption by water and glass.

The reconstructed data are then exported *via* MRC format files to *Amira* 4.1 (Mercury Computer Systems, Carlsbad, CA, USA) for rendering and analysis. In particular, *Amira* was used to extract slices at particular planes through the 3-d volume and to generate 3-d representations including overlays of chemical components. We note that the difference between the 3-d optical density distributions at 532.2 eV and 530.0 eV was performed in *Amira* in order to have high-statistical-precision data for the *IMOD* alignment step. This was a sensible choice in this case owing to the very weak signal from the polyacrylate (<0.025 OD) but more generally, if the chemical signal (from stack fitting of difference maps) is strong, one can carry out the *IMOD* alignment on chemical maps derived in *aXis2000*.

2.5. Spectral processing and chemical mapping

Fig. 3(*a*) shows the structure of the PS/polyacrylate core–shell microspheres (Beach *et al.*, 2005) which were used to demonstrate the technique. Fig. 3(*b*) presents the spectra of the chemical components of the system in the region 527–537 eV, just below the onset of strong absorption by the water and glass (SiO_2) of the capillary. Note the strong peak in the acrylate spectrum owing to the O1*s* $\rightarrow$ π*(C=O) transition that provides a good handle for differentiating the two chemical

components. Even though the C 1*s* spectral region gives an even better chemical differentiation of the two organic components, the pre-O1*s* region is more advantageous for this experiment as the penetration through the sample is much greater. This particular sample was opaque below 320 eV.

3. Results and discussion

3.1. 2-d chemical maps

In a simple two-component system such as this one, chemical identification from NEXAFS data can be determined readily by the difference in images recorded at two energies, in this case at 530 eV and 532.2 eV at the peak of the O 1*s* $\rightarrow$ π*(C=O) transition of the polyacrylate. Alternatively, if images at multiple energies were acquired then chemical maps could be derived by fitting the spectra at each pixel in the image sequence using linear regression procedures such as single value decomposition (SVD) (Pecher *et al.*, 2003). SVD or a closely related stack fit method give chemical maps of one or more components in the sample and can be used on both 2-d or 3-d data. Fig. 4 shows distributions of the chemical components derived from 2-d slices at the center of the capillary. Fig. 4(*a*) shows a map of the PS shells, derived from the aligned 3-d volume at 530 eV [the OD at 530 eV has contributions from all four chemical components (PS, polyacrylate, water, glass), but inside the capillary the PS dominates the structured part of the signal]. Note that the small signal from the acrylate at 530 eV has been ignored since it is expected to be too weak to be detectable, perhaps with the exception of a few specific regions in which the acrylate phase is localized in high concentration as can be seen in Figs. 4(*b*) and 4(*c*). Fig. 4(*b*) shows the same slice of the 3-d map of the
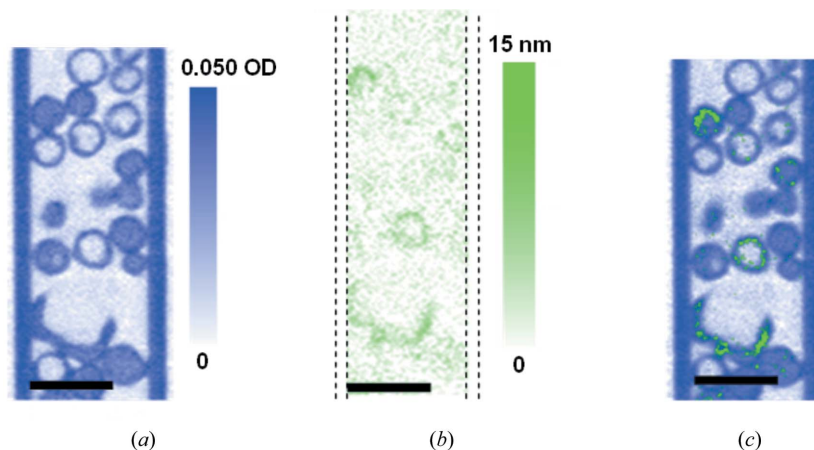

Figure 4
(*a*) Quantitative map of polystyrene, from a slice (50 nm; one voxel thick) through the centre of the capillary extracted from the 3-d volume of 530 eV data. The optical density (OD) scale for the full 3-d data set is derived from the measured transmission intensity using Beers law. This OD scale is preserved through the data processing, thus resulting in a quantitative OD scale for the extracted slice. (*b*) Quantitative map of polyacrylate, from a slice through the 3-d volume of the image differences. The thickness scale is derived from the OD difference signal using the O 1*s* spectrum of polyacrylate plotted in Fig. 3, which was placed on an absolute linear absorbance scale (OD nm^{-1}) by matching the spectrum to the elemental response outside of the structured near-edge region. Since only polyacrylate contributes to the OD difference signal, only the thickness of polyacrylate is obtained. (*c*) A color-coded overlay of the polyacrylate map on the PS map. Scale bar = 2 µm.

polyacrylate, derived from the aligned difference of the signals at the two energies. This difference in optical density per voxel can be described as

$$\Delta \mathrm{OD} = \left[\mu^{\mathrm{PS}}x + \mu^{\mathrm{A}}y + \mu^{\mathrm{W}}z\right]_{532.2} - \left[\mu^{\mathrm{PS}}x + \mu^{\mathrm{A}}y + \mu^{\mathrm{W}}z\right]_{530},$$

where x, y, z is the thickness of PS, acrylate and water, respectively. The change in absorption for PS and water is less than 1% between the two photon energies and is thus neglected,

$$\Delta \mathrm{OD} \simeq \left[\mu^{\mathrm{A}}y\right]_{532.2} - \left[\mu^{\mathrm{A}}y\right]_{530} = 1.86y,$$

and thus the OD scale can be converted into a thickness scale for acrylate. In each case the intensity scale is quantitative since the responses for 1 nm thickness of polyacrylate and PS at solid densities are known to be 0.0028 OD and 0.0011 OD at 532.2 eV (Mitchell *et al.*, 2002; Araki *et al.*, 2006). There are two other chemical components in this system, the glass wall of the capillary, and the water. We have shown elsewhere (Johansson *et al.*, 2006a) that images in the 530–534 eV range are able to differentiate and quantitatively map water and glass, but, since images were recorded at only two photon energies in this case [to minimize the total dose to the easily damaged acrylate (Mitchell *et al.*, 2002)], only two components can be mapped. Analysis of the serum phase suggests that a majority of the polyacrylate electrolyte has leaked out from the spheres and into the serum. However, after dilution by 10000 times, there should be an undetectable amount of acrylate in the serum. Thus most of the apparent signal in the serum phase for Fig. 4(b) is just statistical noise. Fig. 4(c) combines the maps of the two species to indicate more clearly the spatial correlation between these components. Close examination of the composite 2-d slice shows there are cases where there appears to be an accumulation of acrylate in particles on the sides of spheres. There are many other spheres that appear to contain very little acrylate and conversely there appears to be a lower level of acrylate almost homogeneously distributed in the serum phase. The latter is consistent with what was guessed from analysis of dried material, which had also suggested that the spheres have pores that allow the polyelectrolyte to be released into the surrounding aqueous medium.

3.2. 3-d chemical maps

Fig. 5 presents two different 3-d renderings of the combined chemical maps of the PS and polyacrylate components. From the full analysis, the particle structure was spectroscopically determined to have a dense shell comprised of predominately PS and a lower density area comprised of acrylate-containing material. From standard electron microscopy analysis of the dried particles, the shell structure is known to be porous. Owing to this porosity, it was anticipated that the soluble polyacrylate acid solution would be uniformly distributed between the particle interior and serum phase. Surprisingly, the distribution of the acrylate phase was found to be in-homogeneous between the serum phase and particle voids as highlighted in Fig. 5. This finding suggests that the shell
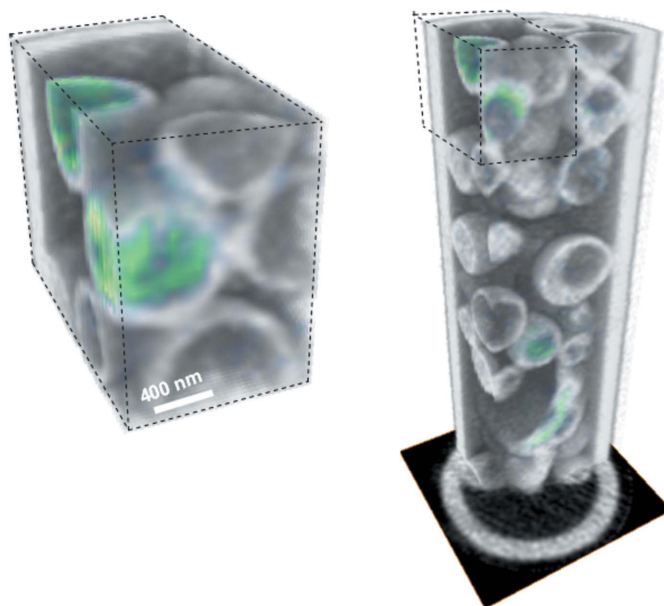

Figure 5
3-d representations of the polyacrylate (green) and polystyrene (gray scale) distributions.

structure is variable across particles. This is the first direct evidence of non-uniform distributions of the acrylate phase in the particle core.

Fig. 6 shows a series of slices through three selected spheres, at 530.0 eV and, thus, predominantly the PS distribution. Sphere 2 has the most typical and expected structure of a PS shell and a hollow inner core for the acrylate solution. Sphere 1 has a surprisingly different structure: it appears to be solid PS. However, it is known that there is a low-density PS strut structure inside some microspheres and perhaps this is over-
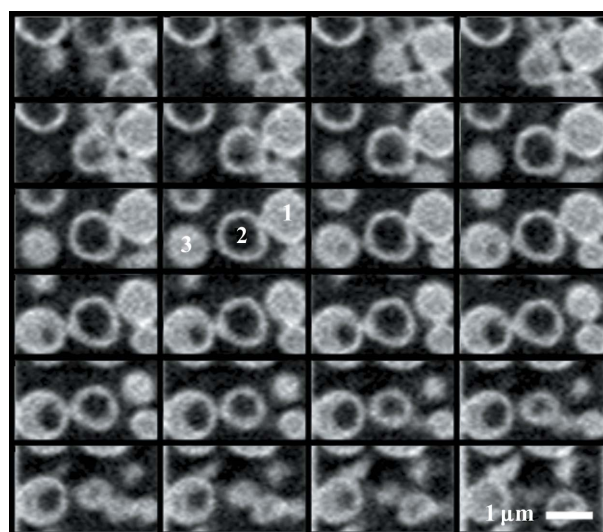

Figure 6
Sequence of 24 2-d slices through a region where three of the microspheres are completely dissected. The sequence starts at the top left and proceeds to the right, then down one row and across to the right and so on. Each 'slice' represents a displacement of 50 nm.

developed in some cases. This may also be an indication that the material was not processed under adequate conditions. Sphere 3 has a non-symmetric interior void. This was the first observation that a portion of the particles are non-symmetric. Clearly the ability to visualize the PS and acrylate distributions in a quasi-independent fashion by multi-energy STXM tomography has given new insights into the microstructure of these materials.

3.3. Evaluation of 3-d resolution and accuracy

The maximum possible resolution and accuracy of the tomographic reconstruction is determined by many parameters. The major factors are the resolution of the acquired 2-d projections and the angular increment between the projections. Secondary factors are how well the alignment procedure succeeded and the severity of artifacts that are added in the back projection. Another important factor is the depth of focus (DOF) of the scanning transmission X-ray microscope. In this study, the 2-d projections (120×240 pixels) of the sample were scanned with 50 nm pixel size using a zone plate (ZP) with 35 nm resolution. The theoretical DOF at the oxygen absorption edge (528–540 eV) is calculated to be 2.1 µm for the ZP (135 µm diameter, 35 nm outer zones) (Attwood, 2000) and photon energies used in this study. This is similar to the sample thickness (2.5 µm), and thus some out-of-focus of the voxels closest and farthest from the zone plate may occur, degrading the resolution slightly. When the stack was acquired, the microscope was refocused at each angle on an interior feature in the capillary to try to minimize this effect. Previous work by Weiß et al. (2000) in full-field transmission X-ray tomography has shown that the 2-d images can be considered close to an ideal projection, with some loss of resolution, for narrow-bandwidth radiation in the case when the DOF is comparable with the sample thickness. The angular increments between the projections were $3°$ and, using the Crowther–DeRosier–Klug formula (Crowther et al., 1970) from electron microscopy tomography, the theoretical resolution limit for this sample owing to the angular sampling is estimated to be 80 nm (pixel size) for a 3 µm-diameter volume. A qualitative test of how successful the image alignment and following tomography reconstruction is to perform a 2-d projection from the 3-d volume and compare it with the original STXM image from the same projection angle. Fig. 7 shows minimal differences between the computer-generated projection (P) and the original STXM projection (O). The misalignment of the images to a common axis of rotation is estimated to be less than or equal to one pixel from a sinogram. In this study the alignment was performed by autocorrelation and by hand, but the *IMOD* software has the capability to utilize fiducial markers, *e.g.* gold beads, that could potentially speed up and increase the accuracy of the alignment.

The accuracy of the quantitative chemical maps of PS and acrylate depends on how well the OD scale can be calibrated for each chemical compound and how much other contri-
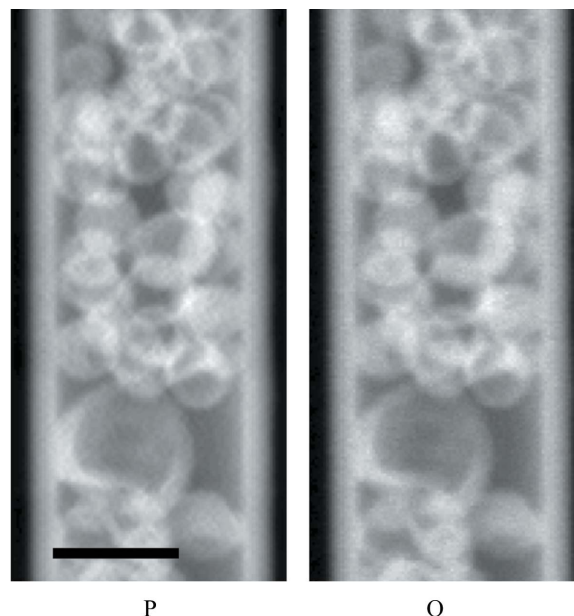

Figure 7
A 2-d projection generated from the computed tomographic reconstruction (P) compared with the original acquired STXM image (O) at the same angle to assess the quality of the reconstruction (scale bar = 2 µm).

buting substances can be suppressed. In many X-ray tomography studies it is customary to use optical densities to identify and map different sample components without using any spectroscopic information. However, that method is inherently inaccurate since it does not take into account any variation of the component density or mixture between components on a subresolution scale. In this study we are using additional spectroscopic information which enables a quantitative chemical mapping for each voxel that is insensitive to variation in component density and mixing of components.

The use of several different software packages for data analysis complicated control of the intensity values and offsets in a consistent and calibrated way. To restore the absolute calibration of the OD scale, three reference conditions were used for the calibration. The first was the absorption through a 50 nm cubic voxel inside the glass capillary wall. The second level used was the absorption through a 50 nm cubic voxel of water in between spheres, where it was assumed that other absorbing components in the water can be neglected. Using previously measured reference spectra (Henke et al., 1993) for water and SiO_2 it was possible to adjust the OD scale to absolute values. The third condition to satisfy was that the optical density histogram for a projection through the reconstructed volume should correspond to the histogram from the original STXM projection. Fig. 4(a) shows a quantitative OD map of a 50 nm-thick slice of the sample at 530.0 eV which is predominantly a PS distribution inside the wall of the glass capillary. In the dense parts of the PS shells the OD reaches close to 80% of solid density of PS. The distribution of acrylate, see Fig. 4(b), shows OD up to 0.025, which corresponds to

about 14 nm thickness at 532.2 eV. The contributions from PS and water in the difference map are much less than 0.5 nm each.

4. Summary and outlook

We have succeeded in chemical mapping a sample of hollow latex particles in the wet state in three dimensions at submicrometer spatial resolution using angle-scan tomography with sample scanning in STXM. This technique has great potential to add useful information about polymer, biological and environmental samples. The time to acquire a tomographic data set with STXM is somewhat longer than that in a full-field transmission X-ray microscope. However, the dose used to acquire this particular sequence was only ~ 200 MGy (500 ms per pixel at a dose rate of ~ 400 MGy s^{-1}, in 1 ms 'acquisitions'), which is considerably lower than typically used in the corresponding full-field tomography (typically 1–10 GGy). Thus the radiation damage of biological and environmental samples often experienced in full-field tomography is expected to be reduced considerably with STXM tomography. We anticipate a further reduction in the radiation damage with implementation of a cryosystem, although this will prove technically challenging if sample scanning is retained, as in this work. With a free-standing sample of appropriate density (*e.g.* 1 µm thick at a solid density of 0.2, as in gels or foams), this technique can be applied even at the C 1s absorption edge, which would significantly further our understanding of biochemical processes occurring in nature. In the future, we will extend the method to studies of 3-d structures of other polymeric systems, which will offer enhancements over our earlier 3-d mapping of toners by serial section STXM (Hitchcock *et al.*, 2003).

References

Ade, H. (1998). *Vacuum Ultraviolet Spectroscopy II, Experimental Methods In The Physical Sciences*, Vol. 32, edited by J. A. R. Samson and D. L. Ederer, pp. 225–261. New York: Academic Press.

Ade, H. & Urquhart, S. G. (2002). *Chemical Applications of Synchrotron Radiation*, edited by T. K. Sham, pp. 285–355. Singapore: World Scientific.

Araki, T., Ade, H., Stubbs, J. M., Sundberg, D. C., Mitchell, G. E., Kortright, J. B. & Kilcoyne, A. L. D. (2006). *Appl. Phys. Lett.* **89**, 124106.

Attwood, D. (2000). *Soft X-rays and Extreme Ultraviolet Radiation, Principles and Applications.* Cambridge University Press.

Baumeister, W., Grimm, R. & Walz, J. (1999). *Trends Cell Biol.* **9**, 81–85.

Beach, E., Keefe, M., Heeschen, W. & Rothe, D. (2005). *Polymer*, **46**, 11195–11197.

Blankenship, R. M. (2001). US Patent 6 252 004 B1.

Clikeman, R. R., Guo, Y., Natoli, J. & Wills, M. C. (1999). US Patent 5 972 363.

Crowther, R. A., DeRosier, D. J. & Klug, F. R. S. (1970). *Proc. R. Soc. London*, **317**, 319–340.

Crowther, R. A., Henderson, R. & Smith, J. M. (1996). *J. Struct. Biol.* **116**, 9–16.

Drobne, D., Milani, M., Zrimecv, A., Lešer, V. & Berden Zrimec, M. (2005). *J. Microsc.* **219**, 219–235.

Dynes, J. J., Lawrence, J. R., Korber, D. R., Swerhone, G. D. W., Leppard, G. G. & Hitchcock, A. P. (2006). *Sci. Total Environ.* **369**, 369–383.

Dynes, J. J., Tyliszczak, T., Araki, T., Lawrence, J. R., Swerhone, G. D. W., Leppard, G. G. & Hitchcock, A. P. (2006). *Environ. Sci. Technol.* **40**, 1556–1565.

Henke, B. L., Gullikson, E. M. & Davis, J. C. (1993). *Atom. Data Nucl. Data Tables*, **54**, 181–342.

Hitchcock, A. P., Araki, T., Ikeura-Sekiguchi, H., Iwata, N. & Tani, K. (2003). *J. Phys. IV*, **104**, 509–512.

Hitchcock, A. P., Morin, C., Zhang, X., Araki, T., Dynes, J. J., Stöver, H., Brash, J. L., Lawrence, J. R. & Leppard, G. G. (2005). *J. Electron Spectrosc. Relat. Phenom.* **144–147**, 259–269.

Hitchcock, A. P., Stöver, H. D. H., Croll, L. M. & Childs, R. F. (2005). *Aust. J. Chem.* **58**, 423–432.

Jacobsen, C., Wirick, S., Flynn, G. & Zimba, C. (2000). *J. Microsc.* **197**, 173–184.

Johansson, G. A., Dynes, J. J., Hitchcock, A. P. Tyliszczak, T., Swerhone, G. D. W. & Lawrence, J. R. (2006a). *Microsc. Microanal.* **12**(Suppl. 2), 1412–1416.

Johansson, G. A., Dynes, J. J., Hitchcock, A. P. Tyliszczak, T., Swerhone, G. D. W. & Lawrence, J. R. (2006b). *Proc. SPIE*, **6318**, 6318–6311.

Jones, C. E., Aviles, R. G., Fasano, D. M. & Vogel, M. (1997). US Patent 5 663 213.

Jurkat-Rott, K. & Lehmann-Horn, F. (2004). *Curr. Pharm. Biotechnol.* **5**, 387–395.

Kilcoyne, A. L. D., Tyliszczak, T., Steele, W. F., Fakra, S., Hitchcock, P., Franck, K., Anderson, E., Harteneck, B., Rightor, E. G., Mitchell, G. E., Hitchcock, A. P., Yang, L., Warwick, T. & Ade, H. (2003). *J. Synchrotron Rad.* **10**, 125–136.

Kotula, P. G., Keenan, M. R. & Michael, J. R. (2004). *Microsc. Microanal.* **10**(Suppl. 2), 1132–1133.

Kowalski, A., Vogel, M. & Blankenship, M. (1984). US Patent 4 427 836.

Kremer, J. R., Mastronarde, D. N. & McIntosh, J. R. (1996). *J. Struct. Biol.* **116**, 71–76.

Larabell, C. A. & Le Gros, M. A. (2004). *Mol. Biol. Cell*, **15**, 957–962.

Lawrence, J. R., Swerhone, G. D. W., Leppard, G. G., Araki, T., Zhang, X., West, M. M. & Hitchcock, A. P. (2003). *Appl. Environ. Microbiol.* **69**, 5543–5554.

Lee, D. I., Mulders, M. R., Nicholson, D. J. & Leadbetter, A. N. (1992). US Patent 5 157 084.

Le Gros, M. A., McDermott, G. & Larabell, C. A. (2005). *Curr. Opin. Struct. Biol.* **15**, 593–600.

McDonald, C. J. & Devon, M. J. (2002). *Adv. Colloid Interface Sci.* **99**, 181–213.

Mastronarde, D. N. (1997). *J. Struct. Biol.* **120**, 343–352.

Mitchell, G. E., Wilson, L. R., Dineen, M. T., Urquhart, S. G., Hayes, F., Rightor, E. G., Hitchcock, A. P. & Ade, H. (2002). *Macromolecules*, **35**, 1336–1341.

Möbus, G. & Inkson, B. J. (2001). *Appl. Phys. Lett.* **79**, 1369–1371.

Pavlyuchenko, V. N., Sorochinskaya, O. V., Ivanchev, S. S., Klubin, V. V., Kriechman, G. S. & Budtov, V. P. (2001). *J. Polym. Sci. Part A Polym. Chem.* **39**, 1435–1449.

Pecher, K., Mccubbery, D., Kneedler, E., Rothe, J., Bargar, J., Meigs, G., Cox, L., Nealson, K. & Tonner, B. (2003). *Geochim. Cosmochim. Acta*, **67**, 1089–1098.

Stöhr, J. (1992). *NEXAFS Spectroscopy, Springer Tracts in Surface Science.* Berlin: Springer.

Stubbs, J. M. & Sundberg, D. C. (2004). *J. Appl. Polym. Sci.* **91**, 1538–1551.

Wang, Y., Jacobsen, C., Maser, J. & Osanna, A. (2000). *J. Microsc.* **197**, 80–93.

Warwick, T., Ade, H., Kilcoyne, D., Kritscher, M., Tylisczcak, T., Fakra, S., Hitchcock, A., Hitchcock, P. & Padmore, H. (2002). *J. Synchrotron Rad.* **9**, 254–257.

Weiß, D., Schneider, G., Niemann, B., Guttmann, P., Rudolph, D. & Schmahl, G. (2000). *Ultramicroscopy*, **84**, 185–197.

Weyland, M. & Midgley, P. A. (2003). *Microsc. Microanal.* **9**(Suppl. 2), 148–149.